Geochemical Perspectives Letters

Europium traces the impact of high temperature hydrothermal systems on the early oceans

S. Viehmann, E.E. Stüeken, S.V. Hohl, N. Tepe, Y. Lin, D. Kraemer, M. Van Kranendonk, J. Krayer, D.M. Ernst, S. Weyer

Supplementary Information

The Supplementary Information includes:

- Samples and Geological Overview
- Analytical Methods, Eu Anomaly Calculation, Sample Screening for Eu_{CN} Seawater Curves, and Description of the Flux Model for Bio-essential Elements
- Supplementary Figures S-1 to S-6
- Supplementary Tables S-1 and S-2
- Supplementary Information References

Samples and Geological overviews

Samples

The samples that were additionally analysed to literature data originate from four IF locations (3.75 Isua IF (Greenland), 3.48 Ga Dresser IF and 3.45 Ga Panorama IF (Australia), 1.88 Ga Gairloch IF (Scotland)) and nine stromatolite locations (3.47 Ga Strelley Pool Fm. (Australia), 2.95 Ga Pongola Supergroup (South Africa), 2.7 Ga Tumbiana Fm. (Australia), 2.2 Ga Hutuo Gr. (China), 1.4 to 1.12 Ga Shennongija Gr. (China), 1.1 Ga Tieling Fm. (China), 1.0 Ga Paranoá Gr. (Brazil), 0.95 Ga Jinshanzhai Fm. (China), 0.55 Ga Dengying Fm. (China)) distributed throughout the Precambrian. Geological overviews of these units are briefly described below. Depositional ages of the IFs and stromatolites of this study and the literature data are taken from the respective publications (see Table S-1).

3.75 Ga old Isua Iron Formation, Greenland

The Eoarchean Isua Greenstone Belt is located in southwest Greenland and comprises >3.7 Ga old iron formations intercalated into greenstone successions (Nutman and Friend, 2009). The area is highly deformed and experienced several up to amphibolite-facies overprints; despite their immense metamorphic history, the trace element composition of the studied IFs has been shown to reflect pristine seawater-like systematics. This study analysed the reference material IF-G from the C.R.P.G. - SARM characterised by (Govindaraju, 1994).

3.48 – 3.45 Ga old Pilbara Iron Formations and stromatolites, Australia

The Palaeoarchean Pilbara Supergroup of the Pilbara Craton, Australia, hosts greenschist-facies greenstone successions with intercalated sedimentary units. The targets of this study are jaspillites from the 3.48 Ga-old Dresser Formation, banded iron formations of the 3.45 Ga-old Panorama Formation, and stromatolitic carbonates from the unconformably overlying Strelley Pool Formation. The Dresser Fm. sediments are interpreted to have formed during severe land-sea transitions (Johnson *et al*., 2022). The slightly younger IFs of the Panorama Fm. have been deposited in a marine caldera

system (Bolhar *et al*., 2005), while the overlying stromatolites formed on an ancient marine carbonate platform (*e.g.*, (Allwood *et al*., 2006)) and preserved pristine seawater-like REE signatures despite intense silicification (*e.g.*, Van Kranendonk *et al*., 2002; Viehmann *et al*., 2020).

2.95 Ga old Pongola stromatolites, South Africa

The Mesoarchean Pongola Supergroup hosts ca. 2.95 Ga old stromatolitic carbonates of the Nzsue Group cropping out in the White Mflozi Inlier of the southeastern Kaapvaal Craton, South Africa. These stromatolites only experienced lower greenschist facies conditions and provided a unique window into microbial habitats due to their remarkable preservation and, thus, were the target of several studies from the interdisciplinary geosciences before (*e.g.*, Eickmann *et al*., 2018; Siahi *et al*., 2018). The stromatolites were formed in a shallow, highly energetic, tide-dominated environment (Siahi *et al*., 2018). Silicification of some stromatolite layers occurred very early because stromatolite chert chips are found in the ambient surrounding carbonate.

2.72 Ga old Tumbiana Formation stromatolites, Australia

The 2.78 to 2.63 Ga old Fortescue Group was deposited in the Hamersley Basin on the Pilbara Craton and contains flood basalts with interbedded chemical and clastic sedimentary successions. One of these intercalated sedimentary successions is the Tumbiana Formation which is dated via U-Pb zircon ages to 2724 ± 5 Ma (Blake *et al*., 2004). Horizons of stromatolitic carbonates of the Meentheena Member have a kilometre-wide lateral extension, can easily recognised on their brownish-black weathering colour throughout the Hamersley Basin, and can be up to 20 m thick (Thorne & Trendall, 2001). The rock successions in this area experienced only low-grade metamorphism (Smith *et al*., 1982) with temperatures not exceeding 300 °C (Lepot *et al*., 2008). The depositional environment of the Tumbiana stromatolites is somewhat debated: most studies argue for a non-marine, possibly ephemeral lake system (*e.g.*, Bolhar & van Kranendonk, 2007; Awramik & Buchheim, 2009). However, some features such as bi-directional sedimentary structures, tidal channels with mud drapes, asymmetric ripples, and aragonite pseudomorphs argue for - at least periodical – marine conditions during deposition of the Meentheena Member (cf. Awramik & Buchheim, 2009).

2.09 Ga old Hutuo Group stromatolites, China

The Paleoproterozoic Hutuo Supergroup on the North China Orogen is prominently outcropping in the area of Mt. Wutai in the Shanxi Province. The base of the Hutuo Supergroup is notably unconformable, resting atop the Neoarchean Gaofan and Wutai Groups. Its sediment thickness exceeds 10.000 meters of excellent outcrop exposures of a storm-dominated shallow marine environment, hosting an abundant and diverse collection of stromatolites (Shixing and Huineng, 1992). Metamorphic overprints only reached sub-greenschist facies, and, thus, marine carbon isotope signatures of the Lomagundi-Jatuli event are excellently preserved in carbonates of the Hutuo Supergroup (Ouyang *et al*., 2020). The domal stromatolites analysed here belong to the Qingshicun Fm. at the boundary of the Dongye and underlying Doucun Subgroups in the Wutai Mountain area that were dated via SHRIMP U-Pb ages from associated tuffs (2087 ± 9; Wilde *et al*., 2004).

1.9 Ga old Gairloch Iron Formation, Scotland

The Palaeoproterozoic meta-volcanic and -sediment series at Gairloch belong to the Loch Maree Group of the Lewsian Gneiss Complex. These units exhibit peak amphibolite facies metamorphic conditions with evidence of retrograde greenschist facies overprints (Park *et al*., 2001). The Loch Maree Group is interpreted to reflect an oceanic plateau with clastic and chemical sediments deposited in relatively shallow water environments. Granodioritic to tonalitic gneisses of the Loch Maree Group were dated to 1903 ± 3 Ma (Park *et al*., 2001).

1.4 Ga old Tieling stromatolites, China

The Mesoproterozic Tieling Formation, North China, overlies the Archean basement and hosts elongated columnar stromatolitic carbonates deposited under high-energy subtidal marine conditions (Tosti and Riding, 2017). The sediments of the Tieling Fm. have undergone Perminan-Cretaceous deformations (Zhang *et al*., 2011), but well-preserved locations occur, for example, at the 1439 ±14 Ma Jixian section (Tosti and Riding, 2017) from which our sample set originates.

1.4 – 1.12 Ga old Shennongija stromatolites, China

The Mesoproterozoic Shennongjia Supergroup hosts over 11 km of marine sedimentary strata deposited on the Yangtze Platform in South China. The Shennongjia Supergroup contains stromatolites with diverse morphologies deposited in shallow shelf environments. Stromatolite samples analysed in this study are taken from the Kuangshishan (<1398 ± 20 Ma), Taizi (1332 ± 67 Ma), Yemahe (1215.8 ± 2.4 Ma) and Shicaohe (1083.2 ± 4.6 Ma) Formations (Zou *et al*., 2019).

1.0 Ga old Paranoà stromatolites, Brazil

Chemical and clastic sediments of the low metamorphic (below greenschist facies) Paranoà Group were deposited on the passive continental margin of the Sao Fransisco Craton. The Paranoà Group unconformably overlies the 1.77 Ga old Araí Group and is also unconformably overlain by the < 0.74 Ga old Jequitai diamictite (Alvarenga *et al*., 2014). Zircon, phosphate, and biostrata ages of the stromatolitic carbonates of this unit point to a depositional age between 1.2 to 1.0 Ga ago. The stromatolites were formed during a transition from a tidal, shallow water environment to a carbonate platform fully connected to the open ocean(Alvarenga *et al*., 2014; Stüeken *et al*., 2022; Viehmann *et al*., 2019).

0.85 Ga old Jinshanzhai stromatolites, China

The Jinshanzhai Fm. at the top of the Huaibei Group (~ 925 to 825 Ma) on the North China Craton consists of 20 m of red shale and reddish-brown small columnar dolomitic stromatolites cropping out below clastic sediments of the Gouhou Fm. including clasts of stromatolite fragments from the underlying Jinshanzhai Fm. (Wan *et al*., 2019; Yang *et al*., 2012). The Jinshanzhai and lower part of the Gouhou Fm are placed in the early Neoproterozoic, verified by detrital zircon U-Pb ages, above the Great Cambrian Unconformity separates the Gouhou Fm. from the Houjiashan Fm. that can be placed by detrital zircon ages into the lower Cambrian (Wan *et al*., 2019). Iron-rich boxonia-type stromatolites have presumably been deposited in an open marine to slightly restricted environment based on carbonate-associated Ba signatures (Hohl *et al*., 2024). Halite pseudomorphs within the Jinshanzhai and Gouhou Fm. argue for hypersaline/evaporative environments at the time of deposition (Wan *et al*., 2019).

0.55 Ga old Dengying stromatolites, China

Stratiform dolomitic stromatolites occur in the Neoproterozoic Dengying Fm. of the Yangtze Platform in South China that conformably overlie black shales of the Doushantuo Formation or sandstones of the stratigraphic equivalent Guanyingya Fm (Zhu *et al*., 2007). Age estimates for the Dengyiang Fm range from 551 Ma to 542 Ma and are derived from the combination of chemo-, biostratigraphy, and chronological dating (*e.g.*, Condon *et al*., 2005). The stromatolites of the Dengying Fm. formed under locally highly oxygenated open-shelf conditions (Ding et al., 2019).

Methods

Analytics and the Eu anomaly calculation

Individual layers of Fe- and Si-rich layers of IFs and jaspers were cut by a diamond-coated saw and milled to homogenous sample powders within an agate ball mill. Iron Formation samples from the Gairloch IF were sampled with a stationary microdriller to produce microdrill cores of the individual layers (2 mm diameter x 20 mm length). Circa 200 mg of sample powder, micro drill cores, and the IF reference material IF-G were digested in high pressure – high-temperature Picotrace digestion blocks at 180 °C for three days in 10 ml of an HCl-HNO_3- HF (3:1:1) mixture. The clear residues were evaporated to incipient dryness and treated twice with 5 ml conc. HCl. After evaporation, the samples were re-dissolved in 3 % HNO_3 for ICP-MS measurements with an Agilent 7900 quadrupole at the University of Vienna and a Perkin Elmer NexION quadrupole at the former Jacobs University Bremen.

Individual stromatolitic carbonate layers were sampled using a diamond-coated hand-held micro-drill. The homogenous sample powders were pre-washed with Milli-Q water or 1 M NaOH, leached with 1 M HAc for 6 to 12 hours in centrifuge tubes, and centrifuged at 4500 RPM. The supernatants of the leached fraction were further diluted for trace element analyses in 2 % HNO_3 and analysed using the Agilent 7900 quadrupole ICP-MS at Tongji University Shanghai.

Europium anomalies are calculated relative to chondrite (subscript CN) with $Eu_{CN}/Eu_{CN}^* = Eu_{CN}/(0.667*Sm_{CN} + 0.333*Tb_{CN})$ with C1 values from (Anders and Grevesse, 1989) rather than to the more commonly used *post-Archean*

Australian shale (PAAS) to avoid positive Eu anomaly artifacts from shale normalisation. Typical features of Archean epiclastic sediments show minor $LREE_{CN}$ enrichment relative to $HREE_{CN}$, flat to strongly depleted $HREE_{CN}$ patterns, and the lack of or the presence of only very small negative Eu_{CN} anomalies (*e.g.*, Taylor and McLennan, 1985, 1995). The latter is a result of the less common fractionation of Eu into feldspars of more evolved rocks which was less abundant in the Archean relative to post-Archean times. Thus, normalising a *post-Archean* shale such as PAAS to chondrite would inevitably result in negative Eu_{CN} anomalies of the shale (Fig. S-1). In turn, normalising to a *post-Archean* shale would then result in an overabundance of Eu_{CN}/Eu_{CN*} ratios as exemplarily shown for the IF reference material IF-G (Fig. S-1). Note, that positive Eu_{CN} anomalies in seawater and its chemical precipitates are a clear seawater signal derived from the presence of high temperature hydrothermal systems that cannot be originated from the chemical weathering of clastic, plagioclase-rich sediments. If this is the case then ambient clastic sediments inevitably must also show the strong positive Eu_{CN} anomalies that are recorded in Archean chemical sediments which is not observed. Anyhow, even modern seawater for which high temperature, hydrothermal systems act as sinks rather than as sources due to immediate REE scavenging onto FeMn (oxyhydr)oxide surfaces close to vent sites (German *et al.*, 1990) shows a positive PAAS-normalised Eu anomaly (*e.g.*, $Eu_{PAAS}/Eu_{PAAS}^* = 1.13$ for Mediterranean seawater; Bau *et al.*, 1997). Thus, we use here chondrite-normalisation of Eu values in marine chemical sediments to avoid this normalisation artifact of the more commonly used shale-normalisation on Eu/Eu* ratios, but give Eu_{CN}/Eu_{CN*} ratios for modern seawater and PAAS in Figs. 1 and 2 of the main text and Fig. S-2 for comparison.

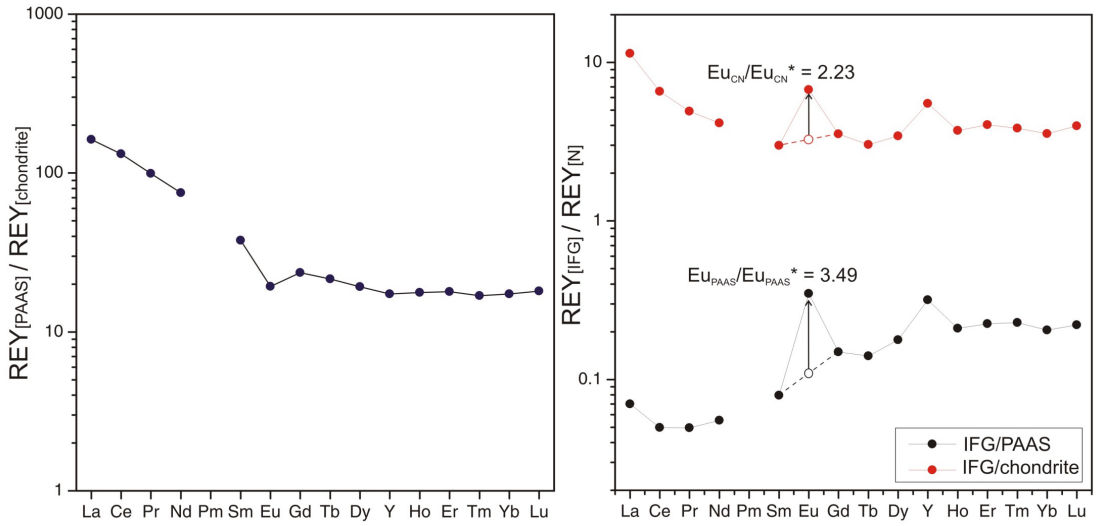

Figure S-1 REE patterns for the post-Archean Australian shale (PAAS) relative to chondrite (left) and IF reference material IF-G normalised to PAAS and chondrite (right). Chondrite-normalised values of *post-Archean* shales such as PAAS show strong LREE enrichment and negative Eu anomalies (left). Thus, normalising to a *post-Archean* shale would result in an overabundance of shale-normalised Eu/Eu* ratios that can be avoided by chondrite-normalisation (right).

Sample selection for the Eu_{CN} seawater curves including a protocol to avoid detrital contamination and post-depositional alteration

The prerequisite for using geochemical fingerprints of marine chemical sediments to reconstruct ancient atmosphere-hydrosphere systematics requires a pure chemical sediment, *i.e.*, a sample that directly reflects the geochemical information derived from seawater. However, syn- (detrital contamination) and post-depositional processes (fluid-rock interactions during diagenesis, metamorphic events, or weathering) may mask and alter the initial geochemical composition from the fluid of which the chemical sediment precipitated.

In this study, we applied a strict protocol and only consider IF and carbonate samples with typical seawater-like REE_{SN} patterns, including positive La_{SN}, Ga_{SN}, Y_{SN} anomalies, and heavy REE_{SN} over light REE_{SN} enrichment, as reliable archives for the Eu distribution through the Precambrian. Notably, typical seawater-like REE_{SN} patterns in stromatolites, of course, exclude stromatolites formed in freshwater and other non-marine settings. We emphasize that only chemical sediments passing this protocol showing typical seawater-like REE_{SN} patterns are used in this study and can reliably be used as archives for Eu systematics in deep and shallow marine settings through the Precambrian.

In the following, the protocol to distinguish between pure chemical sediment samples and those that are affected by post-depositional processes, detrital contamination, BaO interference, and/or experienced REE fractionation processes under non-typical marine conditions is discussed in more detail:

Post-depositional alteration:

Rare Earth's are generally considered very robust against post-depositional alteration processes even in Precambrian chemical sediments such as IFs and stromatolitic carbonates that experienced weak to high metamorphic grades (*e.g.*, Bau, 1993). Bau (1991) proposed that alteration of whole-rock REE patterns during hydrothermal or metamorphic fluid-rock interactions is rather ineffective unless the water-rock ratio is $>>10^2$-10^3 or local metasomatic infiltration is severe. Indeed, Ague (2017) evaluated REE mobility in a variety of metamorphosed rock types in focused fluid flow settings such as veins or lithologic contacts where metasomatic signals are strong. This study observed pristine REE compositions in one-third of the sample set that didn't experience REE mobility. If REE mobility occurred, however, then it typically coincided with fractionation within the REE series and REE incorporation into phosphates and/or garnets. It was also observed that breakdown or growth of plagioclase can deplete and enrich Eu in various rock types, respectively, but during this process, these rocks gained up to 250 % of REE concentrations, showed Eu correlation with Y due to garnet growth, and incorporated strong REE overprinting signatures of the metasomatic fluid (Ague, 2017). Noteworthy, that Eu_{CN}/Eu^*_{CN} ratios considered for Eu curves for IFs and stromatolites in this study show no correlations with P and Y concentrations ($r^2 < 0.1$ for both stromatolites and IF if data are available). This indicates negligible REE distribution into garnets or phosphates and also that plagioclase growth, as well as Eu enrichments during plagioclase breakdown during metamorphic events in the here-considered chemical sediment samples, are insignificant.

Iron Formations (*e.g.*, Appel, 1983, Bolhar *et al*., 2004, Friend *et al*., 2008) and carbonates (Friend *et al*., 2008) of the early Archean Isua supracrustal Belt (Greenland) experienced several up to amphibolite-facies metamorphic overprints but mostly preserved their typical Archean seawater-like shale-normalised (subscript SN) REE_{SN} features such as positive La_{SN}, Gd_{SN}, Y_{SN} anomalies as well as a heavy REE_{SN} over $LREE_{SN}$ enrichment. Similarly, REE can also be robust against carbonate dissolution and re-reprecipitation processes such as observed in silicified stromatolites of the ca. 3.4 Ga old Strelley Pool Fm of the Pilbara Craton (Australia) that almost exclusively consist of re-crystallised dolomite and silica in which the carbonates preserved the typical seawater-like REE_{SN} signatures (*e.g.*, van Kranendonk, 2002; Allwood *et al*., 2010; Viehmann *et al*., 2020). In contrast, associated hydrothermal cherts of the Strelley Pool Fm. show non-seawater-like REE_{SN} patterns and lack all the typical seawater-like REE features (Viehmann *et al*., 2020). This field example is in agreement with studies of, for instance, Banner *et al*., (1988) or Webb *et al*., (2009) showing that REE are very robust during dolomitisation processes because REE reside within the carbonate crystal lattice (Zhong and Mucci, 1995) and a considerable fraction of the carbonate had to be dissolved to change its REE distribution (Banner *et al*., 1988, Webb and Kamber, 2000). It is also observed that (early) Precambrian dolostones and limestones show very similar REE distributions based on different seawater chemistries in Precambrian relative to modern oceans (*e.g.*, Bau and Alexander, 2006). In the Phanerozoic, however, REE_{SN} signatures in contemporaneous limestones and seawater may fairly differ from those of dolostones due to secondary dolomitisation. These observations somehow contradict a recent study by Fralick *et al*. (2024) who reported REE mobility in 2.8 Ga Steep Rock carbonates. While Sr-rich stromatolites show typical seawater-like REE_{SN} patterns with redox-sensitive negative Ce_{SN} anomalies, Sr-poor fenestral stromatolites rich in diagenetic cement and ambient ferroan dolomites lack the negative Ce_{SN} anomaly at still typical seawater-like REE_{SN} patterns. This rare case led the authors to conclude that seafloor diagenetic alteration occurred in the latter rock types by periodic influx of anoxic offshore water masses to overprint the initial negative Ce anomaly. In this case, the carbonate had to be almost completely dissolved and re-precipitated by incorporating the REE geochemistry of the anoxic seawater. The REE in the oxygenated shallow marine water mass and in the anoxic offshore sea masses (which is supposed to have precipitated the ambient IF) is, thus, most likely derived from different sources. To further prove this statement, source proxies such as Sr or Nd isotope compositions of pristine and diagenetically overprinted carbonates and associated IF should be prime targets to confirm and complete the picture.

Anyhow, it is expected that the REE composition of chemical sediments that were altered during low- and high temperature post-depositional fluid-rock interactions during diagenesis, metamorphism or other hydrothermal or supergene enrichment processes will be enriched in light REE during these processes accompanied with a decrease of

the typical seawater-like positive La_{SN}, Gd_{SN} and Y_{SN} anomalies (*e.g.*, William-Jones *et al*., 2012; Gutzmer *et al*. 2008). For instance, light REE enrichment can be observed in a few IF samples from the Isua Greenstone Belt (cf. Frei and Polat, 2007) that indicate post-depositional REE alteration. Louvel *et al* (2022) also proposed increased REE mobility in alkaline hydrothermal fluids as hydroxyl-carbonate complexes that differ fundamentally from those in acidic fluids. The authors showed that LREE are preferentially mobilised by alkaline fluids with temperatures ≥ 400 °C, while HREE are preferentially mobilised in temperature regimes ≤ 200 °C. HREE enrichment in alkaline systems is corroborated by REE studies of modern alkaline lakes that show strong enrichments in $HREE_{SN}$ over $LREE_{SN}$ due to domination of (poly)carbonato-REE complex speciation (e.g., Möller and Bau, 1993; Johannesson and Bird, 1994). If fluids were present in carbonate and IF lithologies, one would expect that REE mobilisation in carbonate succession would enhance REE mobility relative to IF. Additionally, alkaline fluids that reduce and mobilise Eu^{2+} in addition to the other 3+ charged REE should be > 250 °C (Bau, 1993), which would also increase LREE mobility above 400 °C (Louvel *et al*., 2022). However, if REE mobilisation in both rock types related to severe fluid-rock interactions would have occurred at low or high temperatures, the remaining or recrystallised minerals of the carbonates and IFs would then result in REE_{SN} signatures that clearly differ from the typical seawater-like REE_{SN} patterns and anomalies.

In summary, regardless of the potential high or low-temperature modification process(es) of REE in IFs and stromatolitic carbonates, if post-depositional alteration during fluid-rock interactions took place on the REE composition at some stages during Earth's history, the REE signatures would result in non-seawater-like REE signatures and deviate from typical seawater-like REE signals.

Syn-depositional detrital contamination:

Contamination of detrital aluminosilicates that were co-sedimented with the IF or carbonates is a much more common observed phenomenon relative to post-depositional alteration. Clastic contamination modifies the pristine geochemical budget of chemical sediments which is especially important for carbonates and IFs that were deposited close to the ancient coastline and were particularly prone to contamination of subaerial or fluvial transported detrital material. Detrital aluminosilicates such as those derived from volcanic ashes, aeolian processes, or continental weathering show orders of magnitude higher REE concentrations among other almost immobile elements such as Al, Hf, Zr, or Th relative to IFs and carbonates. This concentration difference results in a strong impact of even minute amounts of detrital contamination on the overall geochemical composition of the chemical sediments. This is especially true when the sample material such as IFs and some of the carbonates were fully digested and attacked with a mixture of concentrated HF-HNO_3-HCl in the laboratory (cf. Table S-2). At least for the stromatolitic carbonates, weak HAc leaching partly avoids the digestion of detrital aluminosilicates (cf. Hohl and Viehmann, 2021, and references therein). Anyhow, IFs and carbonates contaminated by different amounts of detrital material are always enriched in REE (and similarly other immobile elements) relative to their pure counterparts and show a wide range of REE concentrations and REE_{SN} patterns. REE_{SN} patterns that are subparallel to modern seawater (with the exception of redox-sensitive Ce and Eu) converge from almost seawater-like in pure chemical sediment endmembers to flat, shale-like REE_{SN} patterns with increasing amounts of detrital contamination (*e.g.*, Nothdurft *et al*., 2004, Viehmann *et al*., 2015) as exemplary shown for the Neoproterozoic Urucum IF (Fig. S-2; Viehmann *et al*., 2016). Notably, even minute amounts of detrital contamination of the chemical sediments lead to a significant decrease of the light REE_{SN} over heavy REE_{SN} enrichment and the positive La_{SN}, $Gd_{SN,}$ and Y_{SN} anomalies, resulting in flatter, non-seawater-like REE_{SN} patterns in chemical sediments that experienced detrital contamination (Fig. S-2).

Thus, detrital contamination of the pristine geochemical REE composition in IFs and carbonates always leads to non-seawater-like REE_{SN} patterns and features and we emphasize that IFs and carbonates showing the typical seawater-like REE signatures *must be* devoid of significant post-depositional alteration processes or detrital contamination that would otherwise result in non-seawater-like REE_{SN} patterns and features.

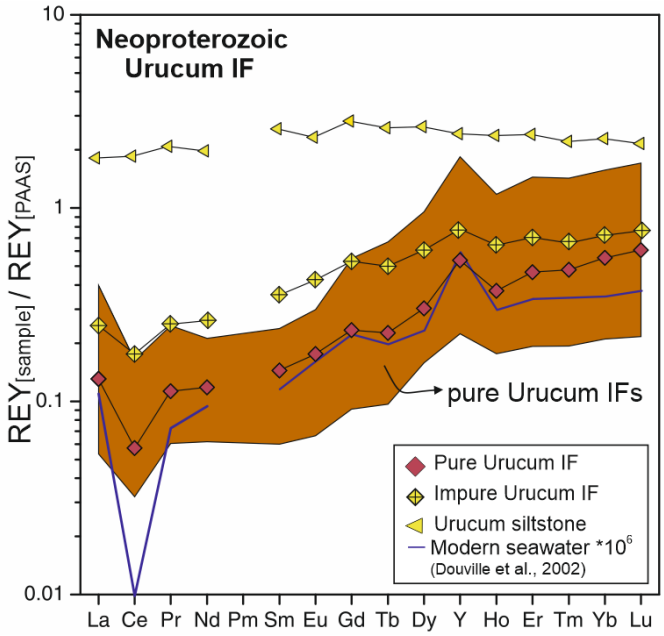

Figure S-2 REE_{SN} patterns of pure IF, detrital contaminated IF samples from the Neoproterozoic Urucum IF relative to those of an ambient shale and modern seawater. The REE_{SN} patterns of pure IF samples that are devoid of detrital contamination are sub-parallel to those of modern seawater. In contrast, IF that are contaminated by variable detrital aluminosilicate contamination show decreasing typical-seawater-like $HREE_{SN}$ over $LREE_{SN}$ enrichment, La_{SN}, Gd_{SN}, and Y_{SN} with increasing REE concertation that eventually converge to the flat patterns observed in the shale (modified after Viehmann *et al*., 2016).

Potential REE fractionation in stromatolite depositional environments

Webb and Kamber (2000) reported REE_{SN} patterns in Holocene reefal microbialites of the Great Barrier Reef and observed that the microbialite REE_{SN} patterns are subparallel to those of ambient open ocean seawater. Based on this study, REE established as an elementary tool to reconstruct paleo-environments of microbial life throughout Earth's history. While it became clear that (stromatolitic) carbonates with seawater-like REE_{SN} patterns formed most likely in a depositional environment connected to the open ocean, many stromatolitic carbonates at different times in Earth's history also show non-seawater-like REE_{SN} patterns that were then related to other depositional environments (cf. Fogret et al., 2014, and references therein). This practice, however, strongly relies on the assumption that REE in stromatolitic carbonates are not fractionated from the ambient water in which the stromatolite formed.

Johannesson *et al*. (2014), however, reported different REE patterns in microbialite carbonates and ambient waters in an extreme environment of a Mexican bolson system and showed that these microbial carbonates do not directly represent ambient water chemistry. The authors propose that fractionation between water and carbonate may be the result of preferential HREE incorporation by organic ligands associated with bacterial cell walls, microbialite biofilms, and/or exopolymeric substances (EPS; Johannesson *et al*., 2014). Organic matter, independent of freshwater, estuarine, or open ocean systems shows almost systematical, relatively flat REE_{SN} patterns with slight middle REE enrichment (Freslon *et al*., 2014). The presence of other particulate surfaces such as authigenic and detrital clays in stromatolite-forming environments (Suosaari *et al*., 2022), the occurrence of lithic and organic nanoparticles (Tepe and Bau, 2014, Merschel *et al*., 2017), and/or water mixing processes between groundwaters and lake/seawater (*e.g.*, Zeyen *et al*., 2021, and references therein) may, however, also be responsible for non-seawater-like REE_{SN} features. Anyhow, regarding the to-date very speculative reasons for REE fractionation in microbial habitats and stromatolite-forming environments, we stress that pure stromatolitic carbonates that formed under open ocean conditions should preserve seawater-like REE_{SN} signatures and can be used as archives to investigate Eu and other REE signatures through deep time. We also want to underscore here that microbial mat systems are very complex bio-geological ecosystems that are far beyond well-understood and that further interdisciplinary research targeting the interactions of geochemical and microbiological processes within the different levels of microbial mats is urgently required for a better understanding of modern and ancient microbial ecosystems.

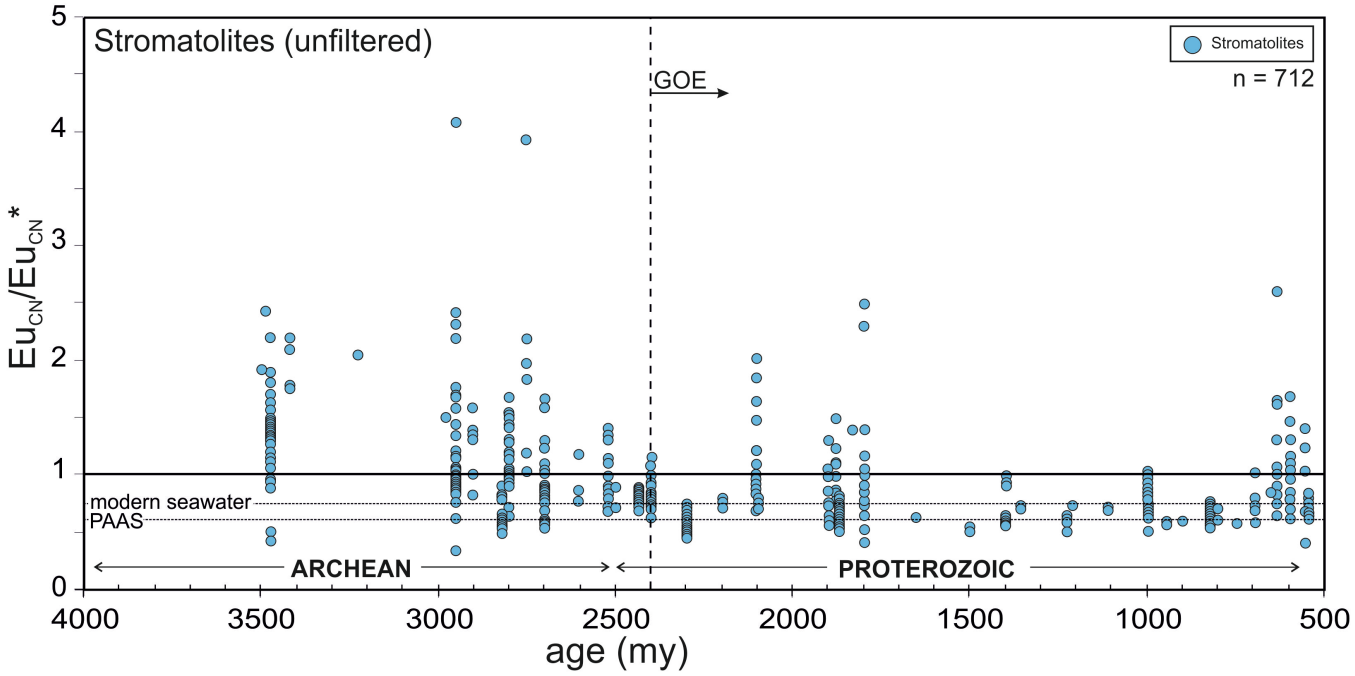

Figure S-3 Precambrian Eu_{CN}/Eu_{CN*} evolution curve of all stromatolites regardless of their depositional setting and Ba/Eu ratios. The average value of Eu_{CN} anomalies in *all* stromatolites (712 data points) shows persistent positive Eu anomalies in Archean samples. In comparison to the filtered graph (Fig. 2 of the main text), however, it becomes obvious that most of the high Eu_{CN}/Eu_{CN*} ratios are a result of BaO interference (Ba/Eu > 3000) rather than a *true* geochemical signal. Percentage values refer to the decrease of Eu_{CN}/Eu_{CN*} values relative to Palaeoarchean stromatolites from the Pilbara Craton. Respective data are given in Table S-2b. GOE: Great Oxidation Event; PAAS: Post Archean Australian Shale.

Impact of BaO interferences:

Screening for published Ba concentrations and positive correlations between Eu_{CN}/Eu_{CN}* and Ba/Eu (see Fig. 2 of the main text for the filtered data and Fig. S-3 for all available stromatolite data regardless of their depositional setting and Ba/Eu ratios) were also applied because high Ba concentrations can lead to artificial Eu_{CN} anomalies based on BaO interferences on Eu during ICP-MS analyses that may significantly affect chemical sediments. This is especially true for carbonates with even lower REE concentrations compared to IFs, and almost all samples showing Ba/Eu ratios over 3000 (Fig. S-4: Viehmann *et al*., 2020) were excluded for interpretation. Figure S-4 also shows that higher REE concentrations of the IFs relative to the stromatolites typically lead to Ba/Eu ratios below the threshold of 3000, suggesting a less pronounced analytical impact on the REE composition of the IF. These observations lead to the inclusion of IF data even without published Ba concentrations.

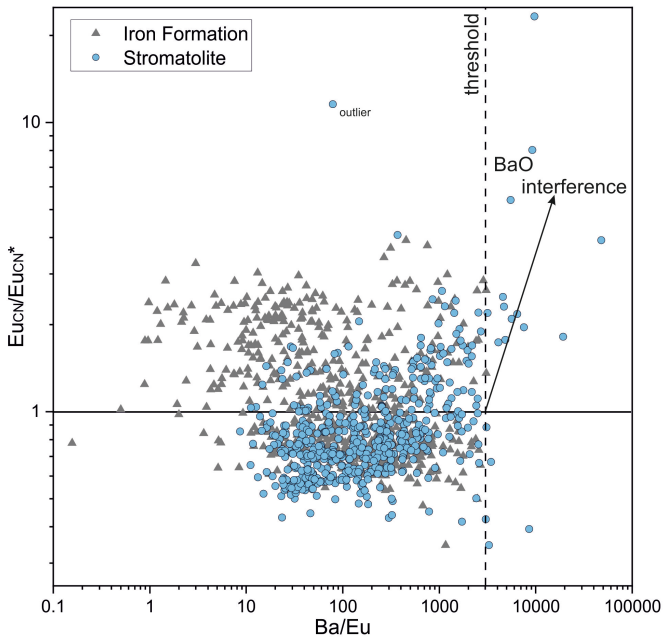

Figure S-4 Eu_{CN}/Eu_{CN*} ratios relative to Ba/Eu ratios of IFs and stromatolites. Eu_{CN}/Eu_{CN*} ratios show no correlations with Ba/Eu until the threshold of ca. Ba/Eu ~ 3000. Over this threshold, analytical BaO interferences on Eu cause a strong increase in Eu_{CN}/Eu_{CN*} ratios that is especially pronounced within carbonates with lower REE concentrations relative to the IFs.

Flux model for bio-essential elements

The modal approach was adopted from (Sander and Koschinsky, 2011) and (Stüeken, 2020), using Geochemist Workbench® (GWB) and the thermo database. Results are shown in figures S-5, S-6, and Fig. 3 of the main text. A black smoker fluid from the modern Rainbow hydrothermal vent field in the mid-Atlantic was used as the hydrothermal endmember. This fluid was mixed with seawater in a ratio from 0.1 to 1000. Modern seawater was taken from (Sander and Koschinsky, 2011). In the Archean scenario, the seawater composition was set to differ from modern seawater in several parameters: pH was set to 7.0 in equilibrium with log(pCO2) = -1.5; the fluid was equilibrated with 10-5 bar H2 instead of 0.21 bar O_2; SO_4^{-2} was reduced to 20 µM; and Fe^{2+} was increased to 100 µM (see (Stüeken, 2020). The mixing calculations were done in the REACT module of GWB. Chloride was used for charge balancing. The maximum step size in the reaction (delxi under Config → stepping) was set to 0.0001. Supersaturated minerals in the hydrothermal fluid were allowed to precipitate prior to mixing, using the 'dump' function. The 'flow-through' function was used to prohibit minerals from back-reacting with the fluid, which is applicable in a scenario where fluid mixing occurs with progressive movement away from the vent center.

In each model, the total number of moles of metals of interest (here Mn, Ni, Co, Cu, and Zn) was monitored. In all cases, some fraction of each metal precipitates upon mixing with seawater. Once precipitation had stopped, we used the final remaining amount of each metal, assuming that this amount would be dispersed into the global ocean. The hydrothermal flux was then calculated by multiplying the metal concentration with a hydrothermal water flux of 1014 L/yr (Reinhard *et al*., 2013).

River concentrations of the five elements were taken from the literature. Henderson and Henderson (2009) report average measured concentrations from modern rivers while (Hao *et al*., 2017) and (Moore *et al*., 2018) calculated river concentrations for the Archean, assuming anoxic conditions and distinct crustal compositions. In both cases, these concentrations were calculated by the modern river water flux of 3.74 x 1016 L/yr (Emerson and Hedges 2008).

We acknowledge that many of the parameters used in this model are uncertain for the Archean ocean. However, the results can provide first-order trends. We find that for all five elements explored in this study, the hydrothermal flux was higher in the Archean than in the modern because a smaller fraction of each element precipitates. This is largely because the low redox state of Archean seawater limits the formation of metal oxides. Furthermore, the lower supply of sulfate impacts the formation of sulfide minerals (Fig. S-6).

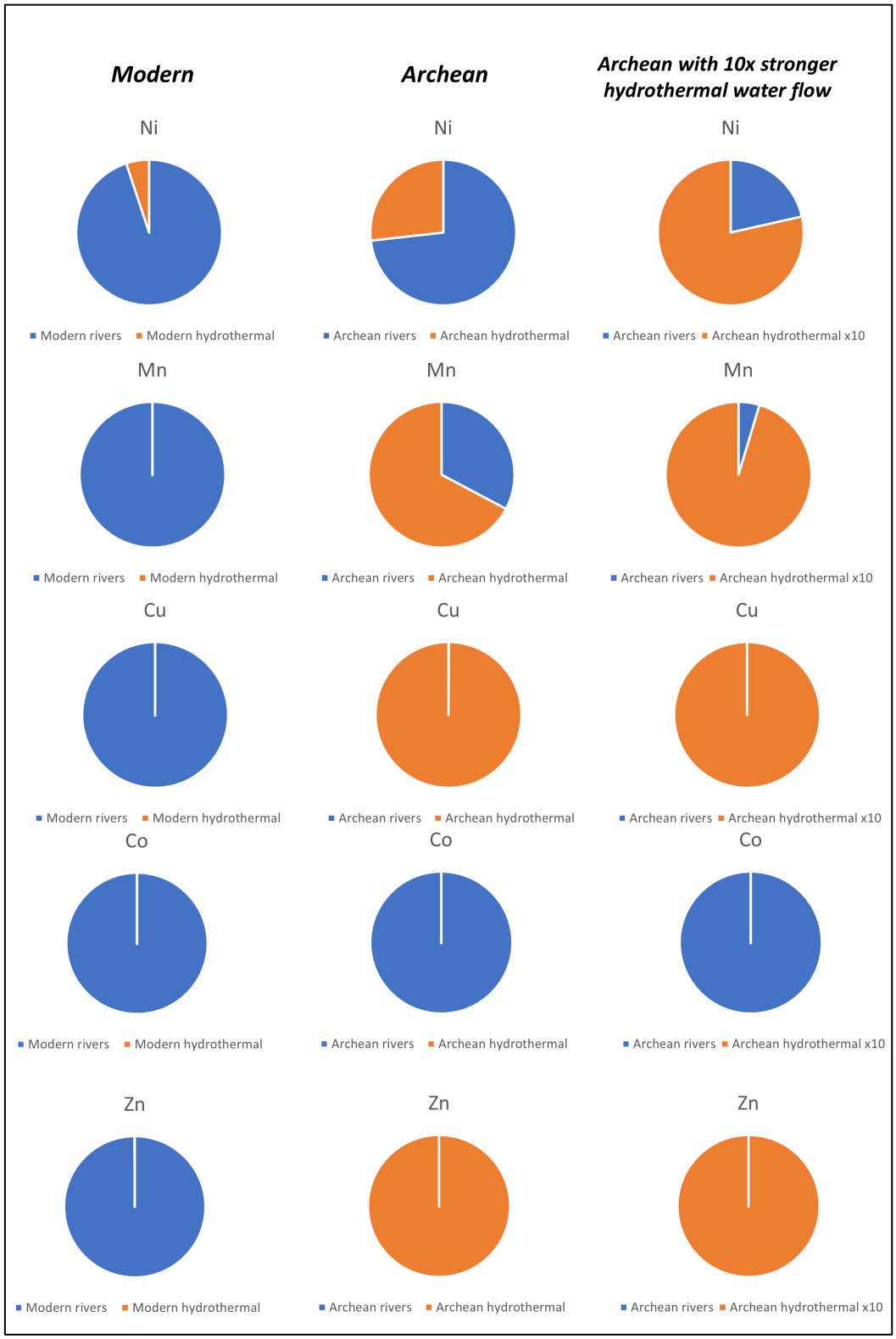

Figure S-5 Estimate of the impact from riverine and hydrothermal sources onto modern and Archean oceans. The results are equivalent to Fig. 3 in the main text but illustrate the proportions of different metal sources relative to each other including an estimation for a 10x stronger hydrothermal flux during Archean times.

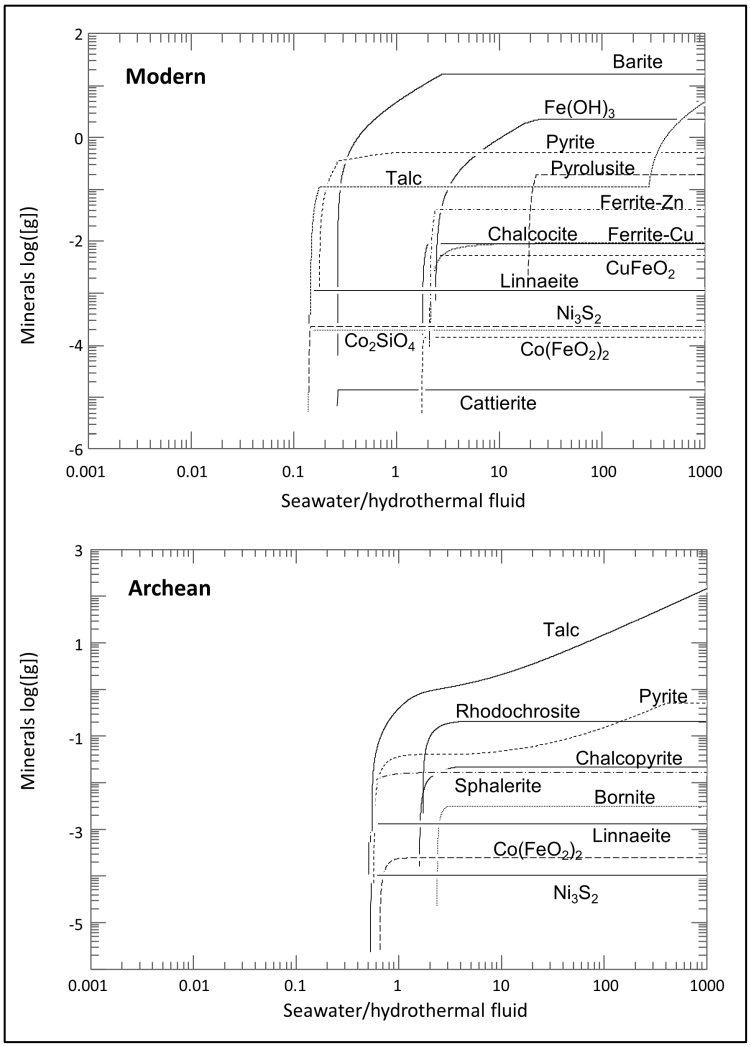

Figure S-6 Precipitation of minerals during mixing of hydrothermal fluid with seawater. Differences in the formation of oxides and sulfides due to differences in seawater composition affect the final concentration of metals that are dispersed into the global ocean.

Supplementary Tables

Table S-1 REE and Ba data of IFs (1a) and stromatolites (1b) from this study.

Table S-2 Eu data of all IFs (2a) and stromatolites (2b) including references.

Tables S-1 and S-2 are available for download (.xlsx) from the online version of this article at http://doi.org/10.7185/geochemlet.2514.

Supplementary Information References

Ague, J.J. (2017) Element mobility during regional metamorphism in crustal and subduction zone environments with a focus on the rare earth elements (REE). *American Mineralogist* 102, 1796–1821. https://doi.org/10.2138/am-2017-6130

Allwood, A.C., Walter, M.R., Kamber, B.S., Marshall, C.P., Burch, I.W. (2006) Stromatolite reef from the Early Archaean era of Australia. *Nature* 441, 714–718. https://doi.org/10.1038/nature04764

Allwood, A.C., Kamber, B.S., Walter, M.R., Burch, I.W., Kanik, I. (2010) Trace elements record depositional history of an Early Archean stromatolitic carbonate platform. *Chemical Geology* 270, 148 - 163. https://doi.org/10.1016/j.chemgeo.2009.11.013

Alvarenga, C.J.S., Santos, R. V., Vieira, L.C., Lima, B.A.F., Mancini, L.H. (2014) Meso-Neoproterozoic isotope stratigraphy on carbonates platforms in the Brasilia Belt of Brazil. *Precambrian Research* 251, 164–180. https://doi.org/10.1016/j.precamres.2014.06.011

Anders, E., Grevesse, N. (1989) Abundances of the elements: Meteoritic and solar. *Geochimica et Cosmochimica Acta* 53, 197–214. https://doi.org/10.1016/0016-7037(89)90286-X

Appel, P.W.U. (1983) Rare earth elements in the Early Archean Isua iron- formation, West Greenland. *Precambrian Research* 20, 243–258. https://doi.org/10.1016/0301-9268(83)90075-X

Awramik, S.M., Buchheim, H.P. (2009) A giant, Late Archean lake system: the Meentheena Member (Tumbiana Formation; Fortescue Group), Western Australia. *Precambrian Research* 174, 215-240. https://doi.org/10.1016/j.precamres.2009.07.005

Banner, J.L., Hanson, G.N., Myers, W.J., (1988) Rare earth element and Nd isotopic variations in regionally extensive dolomites from the Burlington-Keokuk Formation (Mississippian): implications for REE mobility during carbonate diagenesis. Journal of *Sedimentary Petrology* 58, 415-432. https://doi.org/10.1306/212F8DAA-2B24-11D7-8648000102C1865D

Bau, M. (1991) Rare-earth element mobility during hydrothermal and metamorphic fluid-rock interaction and the significance of the oxidation state of europium. *Chemical Geology* 93, 219-230. https://doi.org/10.1016/0009-2541(91)90115-8

Bau, M. (1993) Effects of syn- and post-depositional processes on the rare-earth element distribution in Precambrian iron-formations. *European Journal of Mineralogy* 5, 257–267. https://doi.org/10.1127/ejm/5/2/0257

Bau, M., Alexander, B. (2006) Preservation of primary REE patterns without Ce anomaly during dolomitization of Mid-Paleoproterozoic limestone and the potential re-establishment of marine anoxia immediately after the "Great Oxidation Event". *South African Journal of Geology* 109, 81-86. https://doi.org/10.2113/gssajg.109.1-2.81

Bau, M., Möller, P., Dulski, P. (1997) Yttrium and lanthanides in eastern Mediterranean seawater and their fractionation during redox-cycling. *Marine Chemistry* 56, 123-131. https://doi.org/10.1016/S0304-4203(96)00091-6

Blake, T.S., Buick, R., Brown S.J.A., Barley, M.E. (2004) Geochronology of a Late Archaean flood basalt province in the Pilbara Craton, Australia: constraints on basin evolution, volcanic and sedimentary accumulation, and continental drift rates. *Precambrian Research* 133, 143–173. https://doi.org/10.1016/j.precamres.2004.03.012

Bolhar, R., Kamber, B.S., Moorbath, S., Whitehouse, M.J., Collerson, K.D. (2004) Chemical characterization of earth's most ancient clastic metasediments from the Isua Greenstone Belt, southern West Greenland. *Geochimica et Cosmochima Acta* 69, 1555–1573. https://doi.org/10.1016/j.gca.2004.09.023

Bolhar, R., Van Kranendonk, M.J., Kamber, B.S. (2005) A trace element study of siderite–jasper banded iron formation in the 3.45Ga Warrawoona Group, Pilbara Craton—Formation from hydrothermal fluids and shallow seawater. *Precambrian Research* 137, 93–114. https://doi.org/10.1016/j.precamres.2005.02.001

Bolhar R., Van Kranendonk, M.J. (2007) A non-marine depositional setting for the northern Fortescue Group, Pilbara Craton, inferred from trace element geochemistry of stromatolitic carbonates. *Precambrian Research* 155, 229–250. https://doi.org/10.1016/j.precamres.2007.02.002

Condon, D., Zhu, M., Bowring, S., Wang, W., Yang, A., Jin, Y. (2005) U-Pb Ages from the Neoproterozoic Doushantuo Formation, China. *Science* 308, 95–98. https://doi.org/10.1126/science.1107765

Douville, E., Charlou, J.L., Oelkers, E H., Bienvenu, P., Colon, C.F.J., Donval, J.P., Fouquet, Y., Prieur, D., Appriou, P. (2002) The rainbow vent fluids (36 ° 14′N, MAR): the influence of ultramafic rocks and phase separation on trace metal content in Mid-Atlantic Ridge hydrothermal fluids. *Chemical Geology* 184, 37–48. https://doi.org/10.1016/S0009-2541(01)00351-5

Ding, Y., Chen, D., Zhou, X., Guo, C., Huang, T., Zhang, G. (2019) Cavity-filling dolomite speleothems and submarine cements in the Ediacaran Dengying microbialites, South China: Responses to high-frequency sea-level fluctuations in an 'aragonite–dolomite sea.' *Sedimentology* 66, 2511–2537. https://doi.org/10.1111/sed.12605

Eickmann, B., Hofmann, A., Wille, M., Bui, T.H., Wing, B.A., Schoenberg, R. (2018) Isotopic evidence for oxygenated Mesoarchaean shallow oceans. *Nature Geoscience* 11, 133–138. https://doi.org/10.1038/s41561-017-0036-x

Emerson, S., Hedges, J. (2008) Chemical oceanography and the marine carbon cycle. Cambridge University Press. ISBN: 9780511793202 https://doi.org/10.1017/CBO9780511793202

Fogret, L., Sansjofre, P., Lalonde, S.V. (2024) Geochemistry of carbonate microbialites through time and space: Insights from the microbialite collection of the Muséum National d'Histoire Naturelle (MNHN), France. *Chemical Geology* 662, 122239. https://doi.org/10.1016/j.chemgeo.2024.122239

Fralick, P., Himmler, T., Lalonde, S.V., Riding, R. (2024) Localized geochemical variability produced by depositional and diagenetic processes in a 2.8 Ga Ca-carbonate system: A cautionary paradigm. *Precambrian Research* 410, 107499. https://doi.org/10.1016/j.precamres.2024.107499

Frei, R., Polat, A. (2007) Source heterogeneity for the major components of ~3.7 Ga Banded Iron Formations (Isua Greenstone Belt, Western Greenland): Tracing the nature of interacting water masses in BIF formation. *Earth and Planetary Science Letters* 253, 266–281. https://doi.org/10.1016/j.epsl.2006.10.033

Freslon, N., Bayon, G., Toucanne, S., Bermell, S., Bollinger, C., Chéron, S., Etoubleau, J., Germain, Y., Khripounoff, A., Ponzevera, E., & Rouget, M. L. (2014) Rare earth elements and neodymium isotopes in sedimentary organic matter. *Geochimica et Cosmochimica Acta* 140, 177–198. https://doi.org/10.1016/j.gca.2014.05.016

Friend, C.R.L., Nutman, A.P., Bennett, V.C., Norman, M.D. (2008) Seawater-like trace element signatures (REE + Y) of Eoarchaean chemical sedimentary rocks from southern West Greenland, and their corruption during high-grade metamorphism. *Contributions to Mineralogy and Petrology* 155, 229–246. https://doi.org/10.1007/s00410-007-0239-z

German, C.R., Klinkhammer, G.P., Edmond, J.M., Mitra, A., Elderfield, H. (1990) Hydrothermal scavenging of rare-earth elements in the ocean. *Nature* 345, 516-518. https://doi.org/10.1038/345516a0

Govindaraju, K. (1994) Compilation of working values and sample description for 383 geostandards. *Geostandards Newsletter* 18, 1–158. https://doi.org/10.1046/j.1365-2494.1998.53202081.x-i1

Gutzmer, J., Chisonga, B.C., Beukes, N.J., Mukhopadhyay, J. (2008) The geochemistry of banded iron formation-hosted high-grade hematite-martite iron ores. Economic Geology 15, 157–183. https://doi.org/10.5382/Rev.15.06

Hao, J., Sverjensky, D.A., Hazen, R.M. (2017) A model for late Archean chemical weathering and world average river water. *Earth and Planetary Science Letters* 457, 191–203. https://doi.org/10.1016/j.epsl.2016.10.021

Henderson, P., Henderson, G.M. (2009) The Cambridge Handbook of Earth Science Data. Cambridge University Press, 220 pp. ISBN-13: 9780521693172.

Hohl, S.V., Viehmann, S. (2021) Stromatolites as geochemical archives to reconstruct microbial habitats through deep time: Potential and pitfalls of novel radiogenic and stable isotope systems. *Earth-Science Reviews* 218, 103683. https://doi.org/10.1016/j.earscirev.2021.103683

Hohl, S.V., Lin, Y.B., Wei, H.Z., Wei, G.Y., Viehmann, S. (2024) Barium isotopes in stromatolites through deep-time: A novel tracer for metal cycling in the photic zone. *Earth and Planetary Science Letters* 632, 118639. https://doi.org/10.1016/j.epsl.2024.118639

Johannesson, K.H., Lyons, W.B., Bird, D.A. (1994) Rare earth element concentrations and speciation in alkaline lakes from the western U.S.A. *Geophysical Research Letters* 21, 773–776. https://doi.org/10.1029/94GL00005

Johannesson, K., Telfeyan, K., Chevis, D., Rosenheim, B., Leybourne, M. (2014). Rare Earth Elements in Stromatolites—1. Evidence that Modern Terrestrial Stromatolites Fractionate Rare Earth Elements During Incorporation from Ambient Waters. In: Dilek, Y., Furnes, H. (Eds) Evolution of Archean Crust and Early Life. Modern Approaches in Solid Earth Sciences, vol 7. Springer, Dordrecht.https://doi.org/10.1007/978-94-007-7615-9_14

Johnson, C.M., Zheng, X.Y., Djokic, T., Van Kranendonk, M.J., Czaja, A.D., Roden, E.E., Beard, B.L. (2022) Early Archean biogeochemical iron cycling and nutrient availability: New insights from a 3.5 Ga land-sea transition. *Earth-Science Reviews* 228, 103992. https://doi.org/10.1016/j.earscirev.2022.103992

Lepot K., Benzerara K., Brown G. E., Philippot P. (2008) Microbially influenced formation of 2724-million-year-old stromatolites. *Nature Geosciences* 1, 118–121. https://doi.org/10.1038/ngeo107

Louvel, M., Etschmann, B., Guan, Q., Testemale, D., Brugger, J. (2022) Carbonate complexation enhances hydrothermal transport of rare earth elements in alkaline fluids. *Nature Communications*, 13. https://doi.org/10.1038/s41467-022-28943-z

Merschel, G., Bau, M., Dantas, E.L. (2017) Contrasting impact of organic and inorganic nanoparticles and colloids on the behavior of particle-reactive elements in tropical estuaries: An experimental study. *Geochimica et Cosmochimica Acta* 197, 1–13. https://doi.org/10.1016/j.gca.2016.09.041

Möller, P., Bau, M. (1993) Rare-earth patterns with positive cerium anomaly in alkaline waters from Lake Van, Turkey. *Earth and Planetary Science Letters* 117, 671-676. https://doi.org/10.1016/0012-821X(93)90110-U

Moore, E.K., Hao, J., Prabhu, A., Zhong, H., Jelen, B.I., Meyer, M., Hazen, R.M., Falkowski, P.G. (2018) Geological and Chemical Factors that Impacted the Biological Utilization of Cobalt in the Archean Eon. J*ournal of Geophysical Research: Biogeosciences 123*,3 743–759. https://doi.org/10.1002/2017JG004067

Nothdurft, L.D., Webb, G.E., Kamber, B.S. (2004) Rare earth element geochemistry of Late Devonian reefal carbonates, Canning Basin, Western Australia: confirmation of a seawater REE proxy in ancient limestones. *Geochimica et Cosmochima Acta* 68, 263–283. https://doi.org/10.1016/S0016-7037(03)00422-8

Nutman, A.P., Friend, C.R.L. (2009) New 1:20,000 scale geological maps, synthesis and history of investigation of the Isua supracrustal belt and adjacent orthogneisses, southern West Greenland: A glimpse of Eoarchaean crust formation and orogeny. *Precambrian Research* 172, 189–211. https://doi.org/10.1016/j.precamres.2009.03.017

Ouyang, G., She, Z., Papineau, D., Wang, X., Luo, G., Li, C. (2020) Dynamic carbon and sulfur cycling in the aftermath of the Lomagundi-Jatuli Event: Evidence from the Paleoproterozoic Hutuo Supergroup, North China Craton. *Precambrian Research* 337, 105549. https://doi.org/10.1016/j.precamres.2019.105549

Park, R.G., Tarney, J., Connelly, J.N. (2001) The Loch Maree Group: Palaeoproterozoic subduction–accretion complex in the Lewisian of NW Scotland. *Precambrian Research* 105, 205–226. https://doi.org/10.1016/S0301-9268(00)00112-1

Reinhard, C.T., Planavsky, N.J., Robbins, L.J., Partin, C.A., Gill, B.C., Lalonde, S. V., Bekker, A., Konhauser, K.O., Lyons, T.W. (2013) Proterozoic ocean redox and biogeochemical stasis. *Proceedings of the National Academy of Sciences of the United States of America* 110, 5357–5362. https://doi.org/10.1073/pnas.1208622110

Sander, S.G., Koschinsky, A. (2011) Metal flux from hydrothermal vents increased by organic complexation. *Nature Geoscience* 4, 145–150. https://doi.org/10.1038/ngeo1088

Shixing, Z., Huineng, C. (1992) Characteristics of Palaeoproterozoic stromatolites in China. *Precambrian Research* 57, 1-2, 135-163. https://doi.org/10.1016/0301-9268(92)90097-8

Siahi, M., Hofmann, A., Master, S., Wilson, A., Mayr, C. (2018) Trace element and stable (C, O) and radiogenic (Sr) isotope geochemistry of stromatolitic carbonate rocks of the Mesoarchaean Pongola Supergroup: Implications for seawater composition. *Chemical Geology* 476, 389–406. https://doi.org/10.1016/j.chemgeo.2017.11.036

Smith R.E., Perdrix J.L., Parks T.C. (1982) Burial metamorphism in the Hamersley basin, Western Australia. *Journal of Petrology* 23, 75–102. https://doi.org/10.1093/petrology/23.1.75

Stüeken, E.E. (2020) Hydrothermal vents and organic ligands sustained the Precambrian copper budget. *Geochemical Perspectives Letters* 16, 12–16. https://doi.org/10.7185/geochemlet.2037

Stüeken, E.E., Viehmann, S., Hohl, S.V. (2022) Contrasting nutrient availability between marine and brackish waters in the late Mesoproterozoic: Evidence from the Paranoá Group, Brazil. *Geobiology* 20, 159–174. https://doi.org/10.1111/gbi.12478

Suosaari, E.P., Lascu, I., Oehlert, A.M., Parlanti, P., Mugnaioli, E., Gemmi, M., Machabee, P.F., Piggot, A.M., Palma, A.T., Reid, R.P. (2022) Authigenic clays as precursors to carbonate precipitation in saline lakes of Salar de Llamara, Northern Chile. *Communications Earth and Environment* 3:325. https://doi.org/10.1038/s43247-022-00658-5

Taylor, S.R., McLennan, S.M. (1985) The Continental Crust: Its Composition and Evolution. Blackwell, Oxford, pp. 312.

Taylor, S.R., McLennan, S.M (1995) The geochemical evolution of the continental crust. *Reviews of Geophysics* 33, 241–265. https://doi.org/10.1029/95RG00262

Tepe, N., Bau, M. (2014) Importance of nanoparticles and colloids from volcanic ash for riverine transport of trace elements to the ocean: Evidence from glacial-fed rivers after the 2010 eruption of Eyjafjallajökull Volcano, Iceland. *The Science of the Total Environment* 488–489, 243–251. https://doi.org/10.1016/j.scitotenv.2014.04.083

Thorne A.M., Trendall A.F. (2001) Geology of the Fortescue Group, Pilbara Craton, Western Australia. *Bulletin of the Geological Survey of Western Australia* 144, 1–249.

Tosti, F., Riding, R. (2017) Fine-grained agglutinated elongate columnar stromatolites: Tieling Formation, ca 1420 Ma, North China. *Sedimentology* 64, 871–902. https://doi.org/10.1111/sed.12336

Van Kranendonk, M.J., Hickman, A.H., Smithes, R.H., Nelson, D.R. (2002) Geology and tectonic evolution of the Archean North Pilbara Terrain, Pilbara Craton, Western Australia. *Economic Geology* 97, 695–732. https://doi.org/10.2113/97.4.695

Viehmann, S., Bau, M., Hoffmann, J.E., Münker, C. (2015) Geochemistry of the Krivoy Rog Banded Iron Formation, Ukraine, and the impact of peak episodes of increased global magmatic activity on the trace element composition of Precambrian seawater. *Precambrian Research* 270, 165–180. https://doi.org/10.1016/j.precamres.2015.09.015

Viehmann, S., Bau, M., Bühn, B., Dantas, E.L., Andrade, F.R.D., Walde, D.H.G. (2016) Geochemical characterisation of Neoproterozoic marine habitats: Evidence from trace elements and Nd isotopes in the Urucum iron and manganese formations, Brazil. *Precambrian Research* 282, 74–96. https://doi.org/10.1016/j.precamres.2016.07.006

Viehmann, S., Hohl, S.V., Kraemer, D., Bau, M., Walde, D.H.G., Galer, S.J.G., Jiang, S.-Y., Meister, P. (2019) Metal cycling in Mesoproterozoic microbial habitats: Insights from trace elements and stable Cd isotopes in stromatolites. *Gondwana Research* 67, 101-114. https://doi.org/10.1016/j.gr.2018.10.014

Viehmann, S., Reitner, J., Tepe, N., Hohl, S. V., Van Kranendonk, M., Hofmann, T., Koeberl, C., Meister, P. (2020) Carbonates and cherts as archives of seawater chemistry and habitability on a carbonate platform 3.35 Ga ago: Insights from Sm/Nd dating and trace element analysis from the Strelley Pool Formation, Western Australia. *Precambrian Research* 344, 105742. https://doi.org/10.1016/j.precamres.2020.105742

Wan, B., Tang, Q., Pang, K., Wang, X., Bao, Z., Meng, F., Zhou, C., Yuan, X., Hua, H., Xiao, S. (2019) Repositioning the Great Unconformity at the southeastern margin of the North China Craton. *Precambrian Research* 324, 1–17. https://doi.org/10.1016/j.precamres.2019.01.014

Webb, G.E., Kamber, B.S. (2000) Rare earth elements in Holocene reefal microbialites: a new shallow seawater proxy. *Geochimica Cosmochimica Acta* 64, 1557‑1565. https://doi.org/10.1016/S0016-7037(99)00400-7

Webb, G.E., Nothdurft, L.D., Kamber, B.S., Kloprogge, J.T., Zhao, J.X. (2009) Rare earth element geochemistry of sceletarian coral skeleton during meteoric diagenesis: a sequence through neomorphism of aragonite to calcite. *Sedimentology* 56,1433‑1463. https://doi.org/10.1111/j.1365-3091.2008.01041.x

Wilde, S.A., Zhao, G., Wang, K., Sun, M. (2004) First SHRIMP zircon U-Pb ages for Hutuo Group in Wutaishan: Further evidence for Palaeoproterozoic amalgamation of North China Craton. *Chinese Science Bulletin* 49, 83–90. https://doi.org/10.1007/BF02901747

Williams-Jones, A. E., Migdisov, A.A., Samson, I.M. (2012) Hydrothermal mobilisation of the rare earth elements-a tale of "ceria" and "yttria." *Elements* 8, 355–360. https://doi.org/10.2113/gselements.8.5.355

Yang, D. Bin, Xu, W.L., Xu, Y.G., Wang, Q.H., Pei, F.P., Wang, F. (2012) U-Pb ages and Hf isotope data from detrital zircons in the Neoproterozoic sandstones of northern Jiangsu and southern Liaoning Provinces, China: Implications for the Late Precambrian evolution of the southeastern North China Craton. *Precambrian Research* 216–219, 162–176. https://doi.org/10.1016/j.precamres.2012.07.002

Zeyen, N., Benzerara, K., Beyssac, O., Daval, D., Muller, E., Thomazo, C., Tavera, R., López-García, P., Moreira, D., Duprat, E. (2021) Integrative analysis of the mineralogical and chemical composition of modern microbialites from ten Mexican lakes: What do we learn about their formation? *Geochimica et Cosmochimica Acta* 305, 148–184. https://doi.org/10.1016/j.gca.2021.04.030

Zhang, C.H., Li, C.M., Deng, H.L., Liu, Y., Liu, L., Wei, B., Li, H. Bin, Liu, Z. (2011) Mesozoic contraction deformation in the Yanshan and northern Taihang mountains and its implications to the destruction of the North China Craton. *Science China Earth Sciences 54*, 798–822. https://doi.org/10.1007/s11430-011-4180-7

Zhong, S., Mucci, A. (1995) Partitioning of rare earth elements (REEs) between calcite and seawater solutions at 25°C and 1 atm, and high dissolved REE concentrations. *Geochimica Cosmochimica Acta* 59, 443‑453. https://doi.org/10.1016/0016-7037(94)00381-U

Zhu, M., Zhang, J., Yang, A. (2007) Integrated Ediacaran (Sinian) chronostratigraphy of South China. *Palaeogeography, Palaeoclimatology, Palaeoecology* 254, 7–61. https://doi.org/10.1016/j.palaeo.2007.03.025

Zou, Y., Liu, D., Zhao, F., Kuang, H., Sun, Y., Cheng, J. (2019) Chemostratigraphy of the Mesoproterozoic Shennongjia Group, Yangtze Craton (South China): Implications for oxidized shallow seawaters. *Journal of Asian Earth Sciences* 179, 399–415. https://doi.org/10.1016/j.jseaes.2019.02.026